Experiment 1: Rabbit SAH Model

Drug. An irreversible, broad-spectrum inhibitor for caspases, Z-VAD-FMK (Enzyme Systems Products) was dissolved in 5% DMSO prepared with 0.1 mol/L PBS.

Experimental Design of Rabbit SAH Model. Twenty-four male New Zealand White rabbits weighing between 2.0 and 2.3 kg were randomly assigned to one of the following three groups of eight rabbits each and were subjected to experimental SAH as described later. The rabbits in the SAH-only group underwent SAH without any treatment. The rabbits in the SAH + vehicle group received an injection of vehicle (400 μl of 5% [vol/vol] DMSO in PBS). The animals in the SAH + Z-VAD-FMK group received 1.0 mg of Z-VAD-FMK in 400 μl of 5% DMSO. The dosage of Z-VAD-FMK was determined based on the rabbit meningitis model described elsewhere.[3] A vehicle or Z-VAD-FMK injection was administered intrathecally through the cisterna magna 1 minute before SAH induction.

All rabbits underwent vertebrobasilar angiography 5 days before (baseline) and 2 days after (Day 2) the induction of SAH for the evaluation of cerebral vasospasm. On Day 2, 1.0 ml of CSF was withdrawn from the cisterna magna for Western blot analysis and was immediately centrifuged at 6400 G for 3 minutes and stored at −80°C until use. On Day 2, after assessment procedures were completed, all rabbits were perfusion-fixed with PBS and PBS-containing 4% paraformaldehyde under deep pentobarbital anesthesia. Brains were removed and postfixed overnight in 4% paraformaldehyde at 4°C.

Induction of SAH in Rabbits. The SAH was induced in almost the same fashion as previously described.[28] Briefly, rabbits were anesthetized with ketamine (50 mg/kg intramuscularly) and pentobarbital (20 mg/kg intravenously). The atlantooccipital membrane was exposed through an occipitocervical midline incision. After withdrawal of 1 ml CSF, 2.5 ml of fresh autologous arterial blood was injected into the cisterna magna. Thereafter, rabbits were placed in a head-down prone position for 30 minutes.

Cerebral Angiography. Rabbits were again anesthetized with ketamine (50 mg/kg intramuscularly) and pentobarbital (25 mg/kg intravenously) and received mechanical ventilation through an endotracheal tube. A catheter tip was positioned at the origin of the left vertebral artery via the transfemoral route. By injection of 1 ml of contrast medium through the catheter, angiograms were obtained using a digital subtraction angiography system (Advantex/AMF, GE Co.) at the same magnification for each animal. For strict comparison between pre- and post-SAH diameters, a radiopositive metal was placed beneath the rabbit's head as a reference marker of magnification rate when obtaining angiograms. Arterial blood pressure was recorded on a monitor (Omniace RT3100, NEC Corp.). During the procedures, ventilator adjustments maintained arterial blood pressure and blood gases at standard levels.

Evaluation of Vasospasm in the Rabbit SAH Model. For the evaluation of vasospasm, the diameter of the BA on Day 2 was expressed as a percentage of the baseline diameter before SAH for each rabbit, as we have previously described.[24,28] The mean of diameters at the following three points represents the BA diameter for each angiogram: 0.2 mm above the union of the bilateral vertebral arteries; just below the anterior inferior cerebellar arteries; and 0.2 mm below the top of the BA. Measurements were made in a blinded fashion.

Western Blot Analysis of Rabbit CSF for IL-1β. Stored CSF samples (20 μl) were mixed with a protease inhibitor cocktail (Complete Protease Inhibitor Cocktail, Roche Molecular Biochemicals) and ultracentrifuged at 15,000 G for 15 minutes at 4°C. Supernatants and recombinant rat IL-1β protein (Endogen) were added to the sample buffer (10% glycerol, 0.05 mol/L TRIS-buffered saline [pH 6.8], 10% sodium dodecyl sulfate, and β-mercaptoethanol) in a 2:1 ratio and boiled at 94°C for 4 minutes. Samples and recombinant protein were subjected to electrophoresis in 12.5% sodium dodecyl sulfate–polyacrylamide gels and then transferred onto polyvinylidene difluoride membranes (Hybond-P, Amersham Pharmacia Biotech). After incubation with blocking buffer (5% skim milk in PBS/0.1% Tween 20) overnight at 4°C, the membranes were incubated overnight at 4°C with monoclonal mouse anti-rat IL-1β antibody (R&D Systems) in blocking buffer at a dilution of 2 mg/L, followed by incubation with horseradish peroxidase–linked sheep anti-mouse antibody (Amersham Pharmacia Biotech) for 1 hour at room temperature. Protein bands were detected by an enhanced chemiluminescence method (ECL Plus kit, Amersham Pharmacia Biotech). To confirm specific binding of this antibody for the protein, another membrane was stained in a similar way without the primary antibody.

Histological Examination of Rabbit Brains. For histological examination, all brains were embedded in paraffin and cut into 4-μm sections. They were then stained with H & E and were inspected under a light microscope.

Immunohistochemical Staining in the Rabbit SAH Model. We performed immunohistochemical studies to verify whether and where caspase-1 and its substrate IL-1β were produced during SAH. Nine male New Zealand White rabbits weighing between 2 and 2.3 kg were assigned to one of three following groups (three in each group): an SAH-only, an SAH + vehicle, and an SAH + Z-VAD-FMK group. They were subjected to SAH, treated, and perfusion-fixed, with their brains removed and postfixed, in the same fashion as described earlier. The postfixed rabbit brains were cryoprotected by sequential bathing in 10, 15, 20, and 30% sucrose in PBS at 4°C. They were then snap-frozen in *n*-hexane at −70°C and 8-μm-thick coronal sections were prepared on a cryostat (Cryocut, CM 1850; Leica) at −20°C. The sections were thaw-mounted onto aminoprophyltriethoxysilane-coated slides and stored at −80°C until staining procedures were performed. All incubation steps described in the following section were performed at 4°C and separated by three 5-minute PBS washes.

Peroxidase immunohistochemistry was performed for caspase-1 and IL-1β with commercially available primary antibodies—goat anti–mouse caspase-1 (dilution ratio 1:200; Santa Cruz Biotechnology, Inc.) and goat anti–rabbit IL-1β (dilution ratio 1:200; Endogen). After blocking endogenous peroxidase with peroxidase-blocking reagent (Dako), nonspecific bindings were blocked for 2 hours with 10% normal horse serum in PBS. The sections were then incubated overnight with the primary antibodies in antibody diluent with background-reducing components (Dako) and 0.1% Triton X-100. Sections were then stained with an avidin-biotinylated enzyme complex in which biotinylated secondary antibody, anti–goat IgG (Vectastain ABC kit, Vector Laboratories), was used. The immunoreactive product was visualized with the diaminobenzidine reaction. To assess the specificity of the immunoreactivity, some brain sections were processed as described earlier (the primary antibodies were omitted).

Statistical Analysis

Data for BA diameters in each group were expressed as the mean ± standard deviation, and group differences were tested with analysis of variance followed by a Bonferroni correction. Statistical significance was accepted at a probability value of less than 0.05.

Experiment 2: Rat SAH Model

We evaluated immunoreactivities of caspase-1 and IL-1β in a rat SAH model also, with conventional immunohistochemical and with dual immunofluorescent staining.

Induction of SAH in Rats. Twenty male Sprague–Dawley rats weighing between 350 and 450 g were subjected to SAH under pentobarbital anesthesia (1 mg/kg, intraperitoneally) with basically the same method as in the rabbit SAH model. After withdrawal of 0.1 ml CSF through the atlantooccipital membrane, 0.3 ml autologous arterial blood was injected into the cisterna magna and rats were placed in a head-down prone position for 30 minutes. On Day 2, rats were perfusion-fixed and their brains were postfixed as described in the rabbit SAH model.

Histological Examination of Rats. Ten brains were embedded in paraffin and cut into 4-μm sections. They were then stained with H & E for histological examination under a light microscope.

Immunohistochemical Staining in the Rat SAH Model. The remaining 10 postfixed rat brains were cryoprotected, and frozen sections of these brains were prepared the same way as in the rabbit model.

Peroxidase immunohistochemistry was performed in the same way as in the rabbit model, by using primary antibodies—goat anti–mouse caspase-1 (dilution ratio 1:400; Santa Cruz Biotechnology) and rabbit anti–rat IL-1β (dilution ratio 1:200; Endogen). Sections were stained with an avidin-biotinylated enzyme complex in which biotinylated secondary antibodies were used as follows: anti–goat and anti–rabbit IgG for caspase-1 and IL-1β, respectively (Vectastain ABC kit, Vector Laboratories). To examine the specificity of the immunoreactivity, some brain sections were processed as described earlier (the primary antibodies were omitted).

Dual Immunofluorescent Staining in the Rat SAH Model. For the determination of cellular localization of caspase-1 and IL-1β in macrophages, dual immunofluorescent staining was conducted for either caspase-1 or IL-1β with macrophages. Sections were initially treated with 10% appropriate normal serum in PBS and then incubated overnight with antibody either for caspase-1 or IL-1β in combination with mouse anti–rat macrophage antibody (dilution ratio 1:200; ED-1, Serotec). The same primary antibodies were used at the same dilution as described earlier in conventional immunohistochemical staining for caspase-1 and IL-1β. These primary antibodies were detected in a mixture of fluorophore-labeled secondary antibodies as follows: Green-labeled Alexa Fluor 488 donkey anti–goat IgG conjugate for caspase-1; Green-labeled Alexa Fluor 488 goat anti–rabbit IgG conjugate for IL-1β; and Red-labeled Alexa Fluor 546 goat anti–mouse IgG conjugate for macrophage staining (Molecular Probes), each at a dilution of 1:200. Sections were coverslipped using mounting medium (Prolong Antifade Kit, Molecular Probes), and the fluorophores were then excited and brought to emission. Sections were viewed under a fluorescence microscope (BX50, Olympus).

Results

Experiment 1: Rabbit SAH Model

Cerebral Angiography in Rabbits. Two days after the induction of SAH, the BA diameters were 66.6 ± 3.16% and 66.3 ± 3.74% (mean ± standard deviation) of the baseline diameter in the SAH-only and SAH + vehicle groups, respectively. In contrast, the diameter was 82.6 ± 4.91% in the SAH + Z-VAD-FMK group, showing that Z-VAD-FMK significantly decreased the magnitude of vasospasm (Figs. 1 and 2).

Western Blot Analysis for IL-1β in Rabbit CSF. Bands with a molecular mass of 17 kD, which corresponded to the mature form of IL-1β, were detected in the CSF from rabbits in the SAH-only and SAH + vehicle groups, but not from animals in the SAH + Z-VAD-FMK group (Fig. 3). The membranes without the primary antibody showed no positive bands (data not shown).

Histological Analysis. The BAs exhibited subintimal thickening and severe corrugation of the internal elastic lamina in the SAH-only and SAH + vehicle groups. These morphological changes were far less pronounced in the SAH + Z-VAD-FMK group (data not shown). Many leukocytes infiltrated into the subarachnoid space in all groups. Many of them were mononuclear cells and some took on a

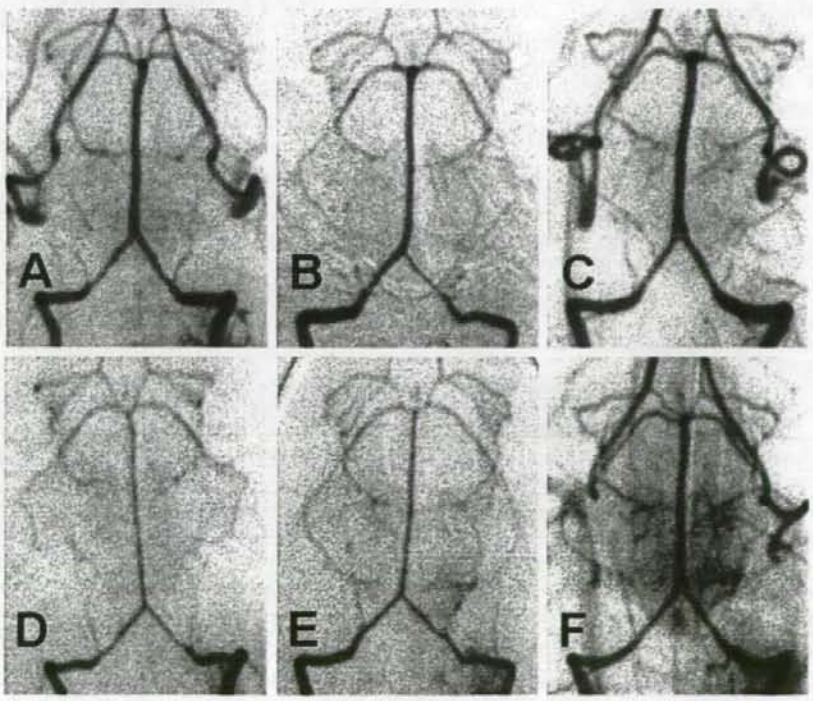

FIG. 1. Representative angiograms obtained in the rabbit SAH model at baseline (A–C) and on Day 2 (D–F) post-SAH. A and D: Angiograms from rabbits in the SAH-only group. B and E: Angiograms from animals in the SAH + vehicle group. C and F: Angiograms from rabbits in the SAH + Z-VAD-FMK group.

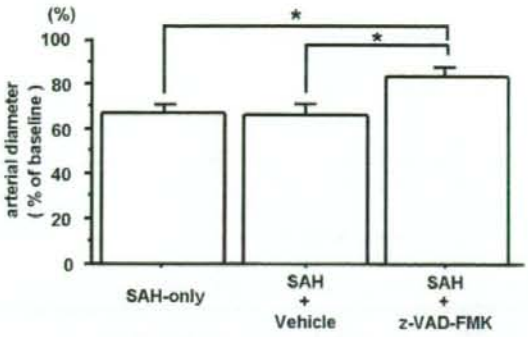

FIG. 2. Bar graph depicting angiographic measurements of the BA diameters 2 days after SAH in rabbits. The degree of arterial narrowing in the SAH + Z-VAD-FMK group is significantly less than that in either the SAH-only or the SAH + vehicle group. * $p < 0.05$.

foamlike appearance and were thought to be phagocytosing macrophages (Fig. 4A and B).

Immunohistochemical Staining for Caspase-1 and IL-1β in the Rabbit SAH Model. In the SAH-only group, immunoreactivities of caspase-1 (Fig. 5A and B) and IL-1β (Fig. 5C and D) were observed in infiltrating large mononuclear leukocytes in the subarachnoid clot, which morphologically corresponded to macrophages. The same immunoreactivities were also observed in the SAH + vehicle group (data not shown). Nevertheless, these immunoreactivities were very scarce in the SAH + Z-VAD-FMK group (data not shown). Omission of the primary antibodies resulted in loss of significant immunoreactivities in the brain sections in all groups (data not shown).

Experiment 2: Rat SAH Model

Histological Analysis. Many leukocytes, including mononuclear cells, infiltrated into the subarachnoid space just like in the rabbit SAH model and many BAs exhibited subintimal thickening and corrugation of the internal elastic lamina, which corresponded to vasospasm (data not shown).

Immunohistochemical Staining for Caspase-1 and IL-1β in the Rat SAH Model. Immunoreactivity of caspase-1 (Fig. 6A and B) and IL-1β (Fig. 6C and D) were observed in mononuclear cells infiltrating the subarachnoid clot. Omission of the primary antibodies resulted in loss of significant immunoreactivities in the brain sections (data not shown).

Dual Immunofluorescent Staining for Caspase-1 and IL-1β in Combination with Macrophages in the Rat SAH Model. Dual immunofluorescent staining for caspase-1 (Fig. 7A) with macrophage (Fig. 7B), and IL-1β (Fig. 7D) with macrophage (Fig. 7E) verified that caspase-1 and IL-1β were expressed in infiltrating macrophages (Fig. 7C and F).

Discussion

The findings in this study are as follows: 1) a caspase inhibitor, Z-VAD-FMK, significantly attenuated cerebral vasospasm in the rabbit SAH model; 2) Western blot analysis confirmed that intrathecal administration of Z-VAD-FMK decreased IL-1β release into the CSF of rabbits affected by SAH; 3) immunoreactivities of caspase-1 and IL-1β were observed in infiltrating mononuclear leukocytes, which morphologically corresponded to macrophages, in the subarachnoid space of rabbits affected by SAH, and these immunoreactivities were suppressed by Z-VAD-FMK; and 4) immunohistochemically proven macrophages infiltrating into the subarachnoid space were immunoreactive for caspase-1 and IL-1β in the rat SAH model. To the best of our knowledge, this is the first immunohistochemical demonstration of the coproduction of caspase-1 and its substrate IL-1β in infiltrating macrophages during SAH.

Of the 14 mammalian caspase family members identified so far,[23] caspase-1 is less involved in the apoptotic cascade but is prominent in inflammation or immune responses because of its pivotal role in regulating the cellular export of proinflammatory cytokines.[10,33] Caspase-1, formerly known as IL-1β–converting enzyme, directly cleaves inactive precursors of IL-1β and IL-18 into their biologically active forms[6,7] and is also reported to play an important role in the production of other proinflammatory cytokines such

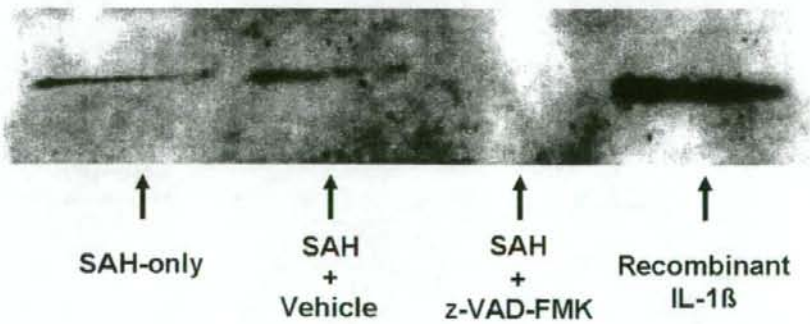

FIG. 3. Western blot analysis of IL-1β in rabbit CSF after SAH. The IL-1β immunoreactivity of a molecular mass of 17 kD is detected in the CSF obtained in the SAH-only and the SAH + vehicle groups, but not in the SAH + Z-VAD-FMK group.

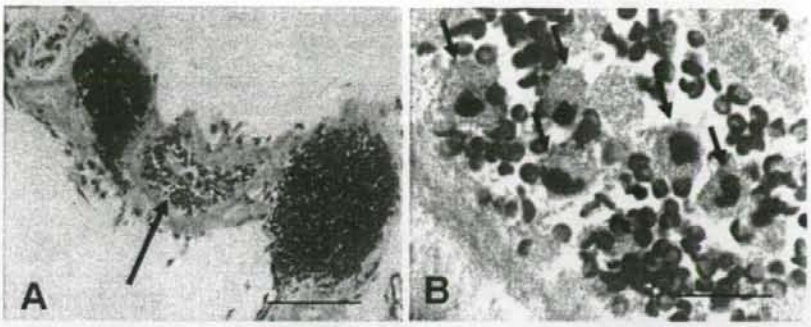

FIG. 4. Representative photomicrographs obtained in the rabbit SAH model. The subarachnoid space is infiltrated with mononuclear cells that have a foamlike appearance, which correspond to phagocytosing macrophages *(arrows)*. H & E, bars = 100 μm (A) and 20 μm (B).

as IL-1α, IL-6, and tumor necrosis factor–α.[17] The expression of caspase-1 has been observed in various kinds of cells such as monocytes[17] and macrophages.[20]

Interleukin-1β is a major regulatory proinflammatory cytokine and a potent inducer for a number of genes, including other cytokines and growth factors, nitric oxide, and prostaglandins.[6] It is known to be synthesized by a wide variety of cells, including monocytes,[17] macrophages,[5] and smooth-muscle cells.[31] Regarding the direct effect of IL-1β on vessel tone, chronic IL-1β application on arteries is reported to induce smooth-muscle hypercontractility through the upregulation of Rho-kinase.[14] As a proinflammatory cytokine, IL-1β induces IL-6 expression in fibroblasts[22] and smooth-muscle cells,[2] IL-1β–deficient mice exhibited reduced production of IL-6 in the setting of inflammation.[8] The cytokine IL-1β stimulates endothelial cells to secrete a potent vasoconstrictor (endothelin-1[34]), is a potent inducer of endothelin receptor expression in vascular smooth-muscle cells, and may be responsible for a generalized activation of the endothelin system.[21] Interleukin-1β is also a major chemoattractant during inflammation and atherogenesis, inducing chemokines such as IL-8 and adhesion molecules such as intercellular adhesion molecule–1 and vascular cell adhesion molecule–1.[4,6] Most of the aforementioned IL-

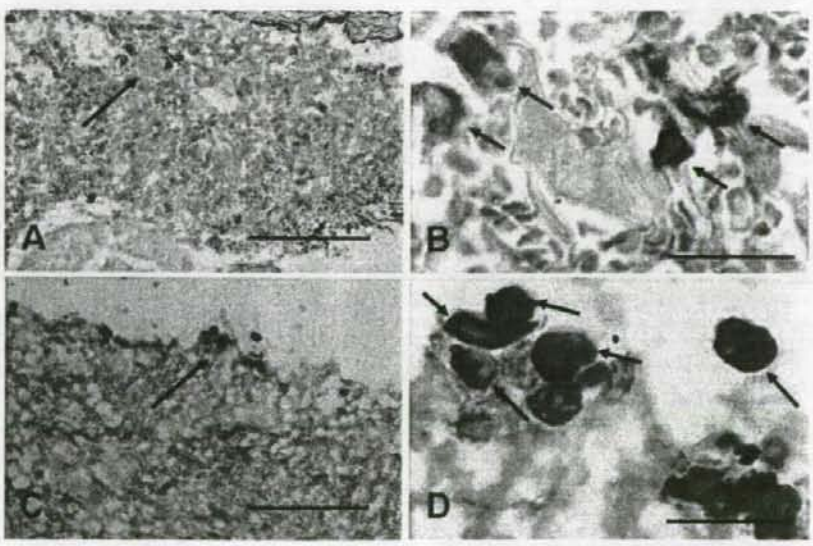

FIG. 5. Immunohistochemical staining obtained in the rabbit SAH model. In the SAH-only group, immunoreactivities for caspase-1 (A and B) and IL-1β (C and D) are observed in mononuclear cells, which morphologically correspond to macrophages infiltrating into the subarachnoid space *(arrows)*. Bars = 100 μm (A and C) and 20 μm (B and D).

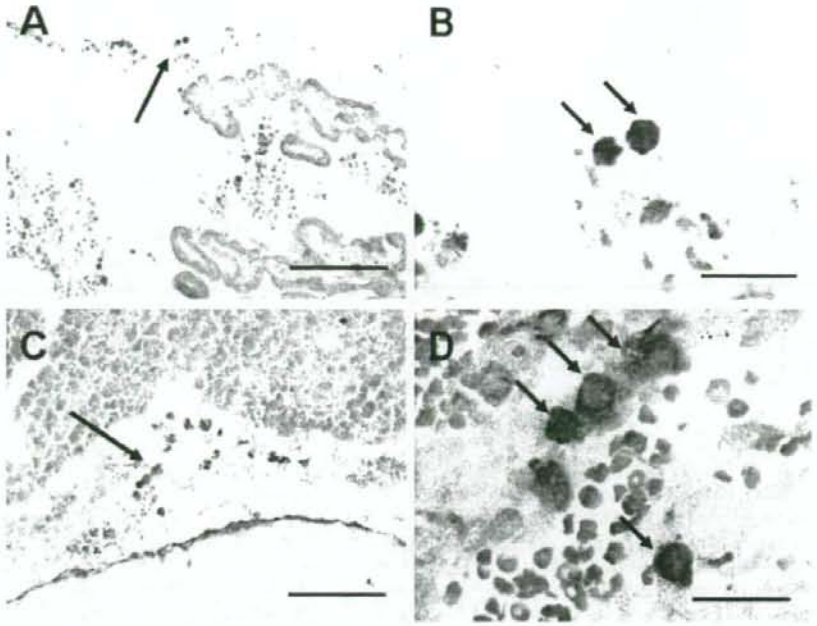

FIG. 6. Immunohistochemical staining obtained in the rat SAH model. Immunoreactivities for caspase-1 (A and B) and IL-1β (C and D) are observed in mononuclear cells infiltrating into the subarachnoid space *(arrows)*. Bars = 100 μm (A and C) and 20 μm (B and D).

1β–stimulated production of proinflammatory molecules is related to the activation of a transcription factor, nuclear factor–κB.[12]

The IL-1β, which is cleaved by caspase-1, and the aforementioned proinflammatory and vasoconstrictive molecules related to IL-1β, have been strongly implicated in the development of SAH-induced vasospasm. The IL-1β is significantly elevated in the CSF of patients with SAH.[9] There is substantial evidence that IL-6, which can cause a long-lasting vasoconstriction, significantly increased in the CSF of patients with SAH and correlated with the incidence of vasospasm.[11,16,19,26] Endothelin-1 has been strongly implicated in vasospasm and its inhibition was reported to ameliorate this condition.[9,36] Adhesion molecules such as intercellular adhesion molecule–1 and vascular cell adhesion molecule–1 were also reported to be elevated in the CSF of patients with SAH,[27] and intracisternal administration of neutralizing antibody against intercellular adhesion molecule–1 significantly reduced vasospasm in a rabbit SAH model.[1] We have previously reported that the intracisternal administration of decoy oligo-DNA against nuclear factor–κB significantly attenuated vasospasm in a rabbit SAH model.[25]

Thus, considering the aforementioned evidence together with our results on Western blot analysis, which demonstrated that Z-VAD-FMK reduced the release of mature IL-1β into the CSF, the antiinflammatory effect of Z-VAD-FMK might lead to a decrease in the severity of vasospasm, inhibiting caspase-1 and its substrate IL-1β, thereby downregulating proinflammatory and vasoconstrictive molecules such as IL-6, endothelin-1, and adhesion molecules. In the present study, we used immunohistochemical assessment to demonstrate the expression of caspase-1 and IL-1β in macrophages infiltrating into the subarachnoid space of rabbits and rats with SAH. In line with our findings, Fassbender et al.[9] showed that coincubation of blood and normal CSF was capable of producing significantly elevated amounts of IL-1β protein, and they also demonstrated that mononuclear leukocytes isolated from bloody CSF in patients with SAH synthesized significantly increased amounts of IL-1β mRNA, concluding that the cellular source of IL-1β in the CSF after SAH is activated mononuclear cells. In our study, Z-VAD-FMK inhibited immunoreactivity of caspase-1 and IL-1β in macrophages infiltrating into the subarachnoid space of rabbits affected by SAH. Therefore, it is conceivable that Z-VAD-FMK attenuated vasospasm by inactivating caspase-1 and subsequently by inhibiting IL-1β production in infiltrating macrophages, and also that infiltrating macrophages may play an important role in the development of vasospasm as a potent producer of various proinflammatory cytokines and vasoconstrictors.

Apoptosis is a process of programmed cell death, in which unnecessary cells are eliminated from multicellular organisms, and is implemented by cascade reactions of the caspase family.[23] Recently Zhou et al.[35] reported that caspase inhibitors attenuated cerebral vasospasm and abolished endothelial apoptosis of cerebral arteries in a dog SAH model, concluding that this antivasospastic effect could result from the inhibition of proapoptotic caspases

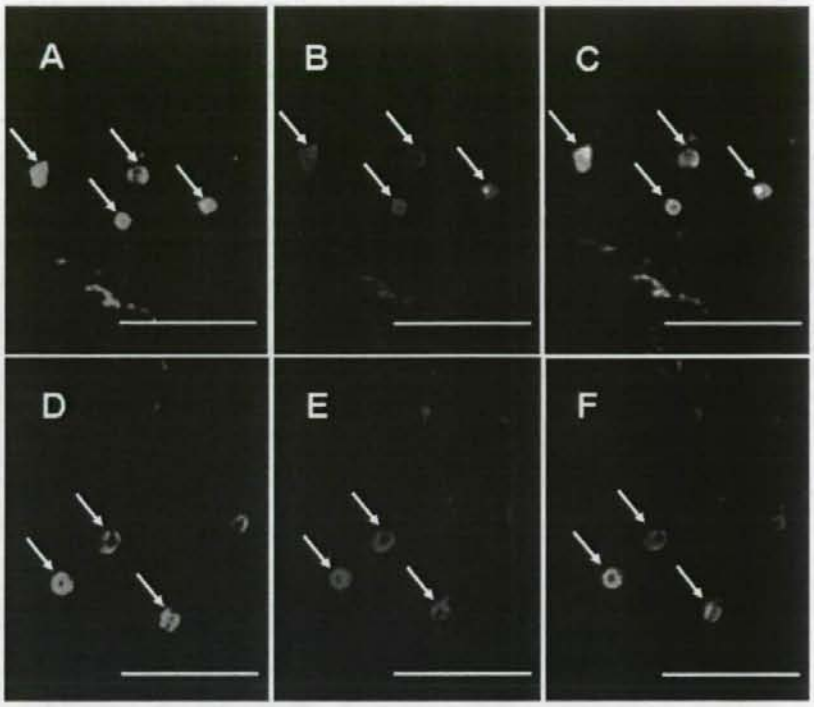

FIG. 7. Dual immunofluorescence staining for either caspase-1 or IL-1β in macrophages obtained in the rat SAH model. Caspase-1 (A, *green*) and IL-1β (D, *green*) immunoreactivities are observed in macrophages stained with a cell marker (B and E, *red*). Merged images are depicted in panels C and F. *Arrows* indicate double-labeled cells. Bars = 50 μm.

such as 3 and 8 in arterial endothelium. Our study has further shown that the antivasospastic effect of caspase inhibitor could also be related to the antiinflammatory effect in the subarachnoid space.

Several studies have recently demonstrated that the inhibition of caspases reduced the infarction size in animal models of cerebral ischemia, making caspase inhibitors candidates for future antiischemic stroke drugs. Intraventricular administration of caspase inhibitors has been shown to reduce the cerebral infarction size in mice and rats.[13] Cerebral ischemia and associated brain edema were reduced in caspase-1–deficient mice.[29] These reports imply that caspase inhibition could also act protectively against the secondary cerebral ischemia resulting from vasospasm.

Conclusions

We demonstrated that the broad caspase inhibitor Z-VAD-FMK attenuated cerebral vasospasm, with the concomitant suppression of IL-1β release into the CSF, and also with the suppression of immunoreactivities of caspase-1 and IL-1β in macrophages infiltrating into the subarachnoid space in a rabbit SAH model. Taken together with another finding of caspase-1 and IL-1β immunoreactivities in immunohistochemically proven macrophages infiltrating into the subarachnoid space in a rat SAH model, this antivasospastic effect of a caspase inhibitor could be related to the inhibition of caspase-1 and IL-1β in macrophages and the eventual downregulation of IL-1β–related proinflammatory and vasoconstrictive molecules. Given the reports that caspase inhibitors work protectively against cerebral ischemia, caspase inhibition could be a viable strategy not only against SAH-induced vascular narrowing itself but also against cerebral ischemia, which is the detrimental consequence of vasospasm.

References

1. Bavbek M, Polin R, Kwan AL, Arthur AS, Kassell NF, Lee KS: Monoclonal antibodies against ICAM-1 and CD18 attenuate cerebral vasospasm after experimental subarachnoid hemorrhage in rabbits. **Stroke 29:**1930–1936, 1998
2. Beasley D: Phorbol ester and interleukin-1 induce interleukin-6 gene expression in vascular smooth muscle cells via independent pathways. **J Cardiovasc Pharmacol 29:**323–330, 1997
3. Braun JS, Novak R, Herzog KH, Bodner SM, Cleveland JL, Tuomanen EI: Neuroprotection by a caspase inhibitor in acute bacterial meningitis. **Nat Med 5:**298–302, 1999
4. Braun M, Pietsch P, Felix SB, Baumann G: Modulation of intercellular adhesion molecule-1 and vascular cell adhesion molecule-1 on human coronary smooth muscle cells by cytokines. **J Mol Cell Cardiol 27:**2571–2579, 1995
5. Davies CA, Loddick SA, Toulmond S, Stroemer RP, Hunt J, Rothwell NJ: The progression and topographic distribution of in-

terleukin-1 beta expression after permanent middle cerebral artery occlusion in the rat. **J Cereb Blood Flow Metab 19:**87–98, 1999
6. Dinarello CA: Biologic basis for interleukin-1 in disease. **Blood 87:**2095–2147, 1996
7. Dinarello CA: Interleukin-1 beta, interleukin-18, and the interleukin-1 beta converting enzyme. **Ann N Y Acad Sci 856:**1–11, 1998
8. Fantuzzi G, Sacco S, Ghezzi P, Dinarello CA: Physiological and cytokine responses in IL-1 beta-deficient mice after zymosan-induced inflammation. **Am J Physiol 273:**R400–R406, 1997
9. Fassbender K, Hodapp B, Rossol S, Bertsch T, Schmeck J, Schutt S, et al: Endothelin-1 in subarachnoid hemorrhage: an acute-phase reactant produced by cerebrospinal fluid leukocytes. **Stroke 31:**2971–2975, 2000
10. Furlan R, Martino G, Galbiati F, Poliani PL, Smiroldo S, Bergami A, et al: Caspase-1 regulates the inflammatory process leading to autoimmune demyelination. **J Immunol 163:**2403–2409, 1999
11. Gaetani P, Tartara F, Pignatti P, Tancioni F, Rodriguez y Baena R, De Benedetti F: Cisternal CSF levels of cytokines after subarachnoid hemorrhage. **Neurol Res 20:**337–342, 1998
12. Han SJ, Ko HM, Choi JH, Seo KH, Lee HS, Choi EK, et al: Molecular mechanisms for lipopolysaccharide-induced biphasic activation of nuclear factor-kappa B (NF-kappa B). **J Biol Chem 277:**44715–44721, 2002
13. Hara H, Friedlander RM, Gagliardini V, Ayata C, Fink K, Huang Z, et al: Inhibition of interleukin 1beta converting enzyme family proteases reduces ischemic and excitotoxic neuronal damage. **Proc Natl Acad Sci U S A 94:**2007–2012, 1997
14. Kandabashi T, Shimokawa H, Miyata K, Kunihiro I, Kawano Y, Fukata Y, et al: Inhibition of myosin phosphatase by upregulated rho-kinase plays a key role for coronary artery spasm in a porcine model with interleukin-1 beta. **Circulation 101:**1319–1323, 2000
15. Kassell NF, Sasaki T, Colohan AR, Nazar G: Cerebral vasospasm following aneurysmal subarachnoid hemorrhage. **Stroke 16:** 562–572, 1985
16. Kikuchi T, Okuda Y, Kaito N, Abe T: Cytokine production in cerebrospinal fluid after subarachnoid haemorrhage. **Neurol Res 17:**106–108, 1995
17. Kuida K, Lippke JA, Ku G, Harding MW, Livingston DJ, Su MS, et al: Altered cytokine export and apoptosis in mice deficient in interleukin-1 beta converting enzyme. **Science 267:**2000–2003, 1995
18. Los M, Wesselborg S, Schulze-Osthoff K: The role of caspases in development, immunity, and apoptotic signal transduction: lessons from knockout mice. **Immunity 10:**629–639, 1999
19. Mathiesen T, Andersson B, Loftenius A, von Holst H: Increased interleukin-6 levels in cerebrospinal fluid following subarachnoid hemorrhage. **J Neurosurg 78:**562–567, 1993
20. McAlindon ME, Hawkey CJ, Mahida YR: Expression of interleukin 1 beta and interleukin 1 beta converting enzyme by intestinal macrophages in health and inflammatory bowel disease. **Gut 42:**214–219, 1998
21. Newman P, Kakkar VV, Kanse SM: Modulation of endothelin receptor expression in human vascular smooth muscle cells by interleukin-1 beta. **FEBS Lett 363:**161–164, 1995
22. Ng SB, Tan YH, Guy GR: Differential induction of the interleukin-6 gene by tumor necrosis factor and interleukin-1. **J Biol Chem 269:**19021–19027, 1994
23. Nunez G, Benedict MA, Hu Y, Inohara N: Caspases: the proteases of the apoptotic pathway. **Oncogene 17:**3237–3245, 1998
24. Ono S, Date I, Nakajima M, Onoda K, Ogihara K, Shiota T, et al: Three-dimensional analysis of vasospastic major cerebral arteries in rats with the corrosion cast technique. **Stroke 28:**1631–1638, 1997
25. Ono S, Date I, Onoda K, Shiota T, Ohmoto T, Ninomiya Y, et al: Decoy administration of NF-kappa B into the subarachnoid space for cerebral angiopathy. **Hum Gene Ther 9:**1003–1011, 1998
26. Osuka K, Suzuki Y, Tanazawa T, Hattori K, Yamamoto N, Takayasu M, et al: Interleukin-6 and development of vasospasm after subarachnoid haemorrhage. **Acta Neurochir (Wien) 140:** 943–951, 1998
27. Polin RS, Bavbek M, Shaffrey ME, Billups K, Bogaev CA, Kassell NF, et al: Detection of soluble E-selectin, ICAM-1, VCAM-1, and L-selectin in the cerebrospinal fluid of patients after subarachnoid hemorrhage. **J Neurosurg 89:**559–567, 1998
28. Satoh M, Date I, Nakajima M, Takahashi K, Iseda K, Tamiya T, et al: Inhibition of poly(ADP-ribose) polymerase attenuates cerebral vasospasm after subarachnoid hemorrhage in rabbits. **Stroke 32:**225–231, 2001
29. Schielke GP, Yang GY, Shivers BD, Betz AL: Reduced ischemic brain injury in interleukin-1 beta converting enzyme-deficient mice. **J Cereb Blood Flow Metab 18:**180–185, 1998
30. Thornberry NA, Lazebnik Y: Caspases: enemies within. **Science 281:**1312–1316, 1998
31. Wang X, Romanic AM, Yue TL, Feuerstein GZ, Ohlstein EH: Expression of interleukin-1 beta, interleukin-1 receptor, and interleukin-1 receptor antagonist mRNA in rat carotid artery after balloon angioplasty. **Biochem Biophys Res Commun 271:** 138–143, 2000
32. Weir B, Macdonald RL, Stoodley M: Etiology of cerebral vasospasm. **Acta Neurochir Suppl 72:**27–46, 1999
33. Wong WW: ICE family proteases in inflammation and apoptosis. **Agents Actions Suppl 49:**5–13, 1998
34. Yoshizumi M, Kurihara H, Morita T, Yamashita T, Oh-hashi Y, Sugiyama T, et al: Interleukin 1 increases the production of endothelin-1 by cultured endothelial cells. **Biochem Biophys Res Commun 166:**324–329, 1990
35. Zhou C, Yamaguchi M, Kusaka G, Schonholz C, Nanda A, Zhang JH: Caspase inhibitors prevent endothelial apoptosis and cerebral vasospasm in dog model of experimental subarachnoid hemorrhage. **J Cereb Blood Flow Metab 24:**419–431, 2004
36. Zimmermann M, Seifert V: Endothelin and subarachnoid hemorrhage: an overview. **Neurosurgery 43:**863–876, 1998

Manuscript submitted April 30, 2006.
Accepted January 9, 2007.
Dr. Date holds a grant from the Ministry of Education, Science, Sports, and Culture, Japan; Special Coordination Funds of the Science and Technology Agency of the Japanese government; and Health Sciences Research grants for research on brain science.

Address reprint requests to: Keiichi Iseda, M.D., Department of Neurological Surgery, Okayama University Graduate School of Medicine, Dentistry, and Pharmaceutical Sciences, 2-5-1 Shikata-cho, Okayama 700-8558, Japan. email: keiiseda@pop21.odn.ne.jp.

Surg Today (2007) 37:412–417
DOI 10.1007/s00595-006-3423-2

SURGERY TODAY

Case Reports

Pseudoaneurysm of the Cystic Artery Secondary to Cholecystitis as a Cause of Hemobilia: Report of a Case

TOMOTAKA AKATSU, MINORU TANABE, TOMOHIRO SHIMIZU, KAN HANDA, SHIGEYUKI KAWACHI, KOICHI AIURA, MASAKAZU UEDA, MOTOHIDE SHIMAZU, and MASAKI KITAJIMA

Department of Surgery, Keio University School of Medicine, 35 Shinanomachi, Shinjuku, Tokyo 160-8582, Japan

Abstract
Spontaneous intracholecystic bleeding is very rare. We report herein a very rare case of a pseudoaneurysm of the cystic artery due to acute cholecystitis. A 58-year-old man presented at the emergency department complaining of colicky pain in the right upper quadrant. Dynamic magnetic resonance imaging demonstrated an early-enhanced pooling of contrast material (suggestive of a pseudoaneurysm of the cystic artery) inside the neck of the gallbladder. After the proximal control of the hepatic artery, the patient underwent a cholecystectomy and a ligation of the cystic artery. The resected specimen of the gallbladder showed evidence of a massive intracholecystic hematoma. Proximal to the impacted gallstone in the neck, a 2-cm diameter saccular-type pseudoaneurysm was identified. Although a pseudoaneurysm of the cystic artery is very rare, it should be included in the differential diagnosis of hemobilia. Once the pseudoaneurysm is confirmed, its embolization before a cholecystectomy (which can be attempted laparoscopically) may be useful to ensure the safety of the patient.

Key words Pseudoaneurysm · Cystic artery · Cholecystitis · Hemobilia · Gallbladder

Introduction

Gastrointestinal bleeding from the biliary tree, termed "hemobilia," is an uncommon event.[1,2] The most common cause of this disease, iatrogenic or traumatic liver injury, accounts for approximately half of all cases.[3,4] Recently, hemobilia has also been reported as a complication after a laparoscopic cholecystectomy.[5–8] Spontaneous intracholecystic bleeding is very rare, and it has been described in patients with vascular diseases (such as polyarteritis nodosa), blood coagulation disorders (such as hemophilia and von Willebrand's disease), hepatic or biliary tumors, and parasite infection.[9–11] We report here a very rare case of a pseudoaneurysm of the cystic artery due to acute cholecystitis.

Reprint requests to: T. Akatsu
Received: September 27, 2006 / Accepted: December 4, 2006

Case Report

A 58-year-old man presented to the emergency department complaining of colicky pain in the right upper quadrant. He had been experiencing occasional right hypochondoralgia for 2 weeks. He denied any history of trauma or recent surgery. The patient was febrile and jaundiced with diffuse tenderness in the upper abdomen and normal blood pressure. Since undergoing bilateral nephrectomies for renal cell carcinomas associated with sclerotic kidney 3 years earlier, he had been receiving dialysis treatment three times a week.

The laboratory test results included white blood cell count of 11900/mm^3, a hemoglobin level of 10.3 g/dl, and platelet count of 329000/mm^3. Biochemical tests demonstrated the presence of aspartate aminotransferase at 928 IU/l (normal 10–35 IU/l), alanine aminotransferase at 671 IU/l (normal 5–40 IU/l), alkaline phosphatase at 1853 IU/l (normal 100–320 IU/l), γ-glutamyltransferase at 523 IU/l (normal 5–40 IU/l), total bilirubin (T-Bil) at 3.4 mg/dl (normal 0.4–1.4 mg/dl), and amylase at 214 IU/l (normal 57–145 IU/l). His coagulation test results were within the normal limits.

Ultrasonography (US) and contrast-enhanced computed tomography (CT) showed a distended, thick-walled gallbladder filled with irregular-shaped masses (suggestive of hematoma). A large gallstone was present. Nonetheless, no cause for an intracholecystic hemorrhage was evident at this time. These radiologic

findings suggested that the patient had acute cholecystitis. Nevertheless, due to the presence of right upper quadrant pain, fever, and abnormal liver function tests, cholangitis was thought to be a likely diagnosis. To decompress the gallbladder, a percutaneous transhepatic gallbladder drainage tube (8F) was inserted under local anesthesia. Dark-red bloody bile was evacuated, and a culture of the bile demonstrated *Staphylococcus epidermidis*, which suggested cholecystitis. Cholangiography via the drainage tube showed irregular-shaped filling defects and gallstone impaction in the neck of the gallbladder (Fig. 1A). Side-view endoscopy showed blood oozing from the papilla of Vater (Fig. 1B). Endoscopic retrograde cholangiography (ERCP) demonstrated filling defects to also be present in the common bile duct, and therefore a nasobiliary drainage tube (5F) was placed in it for temporary decompression before surgery. Dynamic magnetic resonance imaging (MRI) demonstrated an early-enhanced pooling of contrast material (suggestive of a pseudoaneurysm of the cystic artery) inside the neck of the gallbladder (Fig. 1C). A cholecystectomy, including an excision of the pseudoaneurysm, was thus planned.

At laparotomy, the gallbladder was found to firmly adhere to the omentum. The hepatic artery was secured in preparation for serious and uncontrolled bleeding. Because strong pericholecystic adhesion prevented proper orientation around Calot's triangle, the gallbladder was thus dissected from the liver bed. After mobilization of the gallbladder from the liver bed and hepatoduodenal ligament, intraoperative US confirmed the presence of a pseudoaneurysm inside the neck of the gallbladder. The cystic artery was dissected carefully and ligated, then the gallbladder was removed. Intraoperative cholangiography showed no biliary tree abnormalities. The nasobiliary drainage tube was left in place.

The resected specimen of the gallbladder showed evidence of a massive intracholecystic hematoma (Fig. 2A). Proximal to the impacted gallstone in the neck, a 2-cm diameter saccular-type pseudoaneurysm was thus identified (Fig. 2B). Microscopically, the aneurysmal dilation was found to communicate with the interrupted cystic artery inside the severely inflamed gallbladder wall (Fig. 3A–C), suggesting that cholecystitis led to the pseudoaneurysm formation of the cystic artery. The gallbladder mucosa was breached in many places, and inflammatory cells infiltrated prominently into the wall of the gallbladder. There was also no evidence of malignancy. A pseudoaneurysm of the cystic artery associated with acute calculous cholecystitis was the final diagnosis.

Postoperatively, the patient's jaundice improved. He recovered uneventfully and thus was discharged. He was alive and well 12 months after surgery.

Discussion

We herein reported a unique case of hemobilia caused by pseudoaneurysm of the cystic artery. In the present case, acute cholecystitis led to pseudoaneurysm forma-

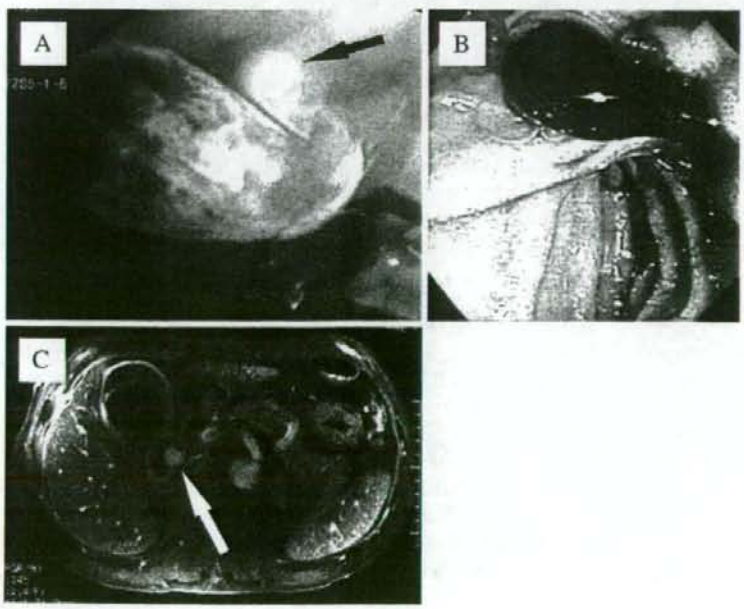

Fig. 1. A Cholangiography via a percutaneous transhepatic gallbladder drainage tube showing irregular-shaped filling defects (intracholecystic hematoma) and gallstone impaction in the neck (*arrow*). **B** Side-view endoscopy demonstrating blood oozing from the papilla of Vater. **C** Dynamic magnetic resonance imaging showing an early-enhanced pooling of contrast material inside the neck of the gallbladder (*arrow*) in the same manner as in the abdominal aorta

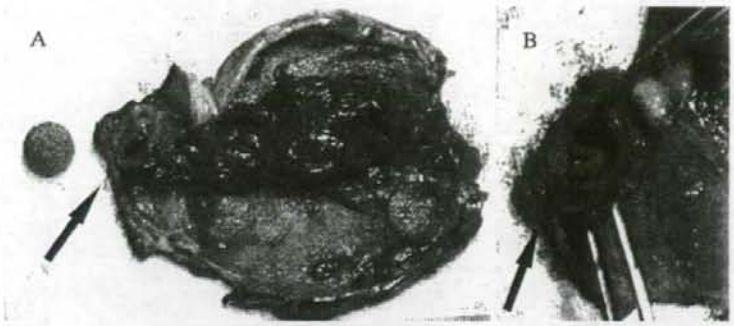

Fig. 2A,B. The resected specimen of the gallbladder. **A** A massive hematoma was present inside the gallbladder. Next to the gallstone, which was impacted in the neck, a saccular-type pseudoaneurysm measuring 2 cm in diameter (*arrow*) was identified. **B** The cut section of the aneurysm (*arrow*) showing no normal vascular structures

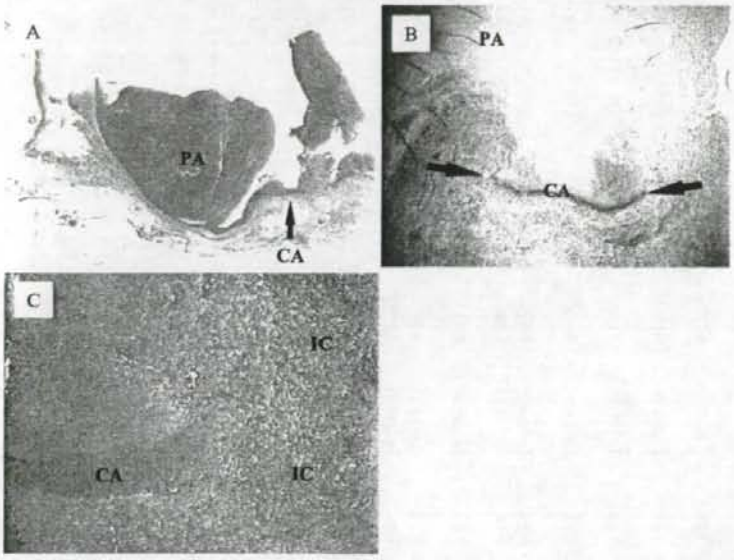

Fig. 3A–C. Microscopic findings. **A** The pseudoaneurysm communicates with the cystic artery. *PA*, pseudoaneurysm; *CA*, cystic artery. **B** The tunica elastica externa (*arrows*) of the cystic artery is interrupted. *PA*, pseudoaneurysm; *CA*, cystic artery. **C** Inflammatory cells infiltrate the wall of the gallbladder around the cystic artery. *CA*, cystic artery; *IC*, inflammatory cells

tion in the gallbladder, which later bled internally. This case was successfully treated by external drainage of the gallbladder and the common bile duct, followed by a cholecystectomy with proximal control of the hepatic artery.

A pseudoaneurysm of the cystic artery due to acute cholecystitis is very rare. In a PubMed search of the literature (using key words pseudoaneurysm, cystic artery, and cholecystitis), only 15 such cases have been identified in the English literature (Table 1).[12-26] One case of a cystic artery pseudoaneurysm caused by pancreatitis was excluded.[27] The 16 cases (including the present case) consisted of 11 men and 5 women whose ages ranged from 32 to 73 years (median, 65 years). Hemobilia generally presents as upper quadrant pain (biliary colic), obstructive jaundice, and gastrointestinal hemorrhaging (Quincke's triad). Nine of the 16 cases (56%) demonstrated the triad. In 56% of the cases (9/16), the pseudoaneurysm was located inside the gallbladder [the remaining 44% (7/16) of pseudoaneurysms were outside the gallbladder]. The pseudoaneurysms ranged in size from 0.2 cm to 4 cm (median, 2.5 cm). There was a single gallstone in eight cases and multiple stones in four cases. Gallstone impaction in the neck was noted in 4 (27%) of 15 cases (in one case no data were available). Fifteen cases underwent a cholecystectomy with ($n = 4$) or without ($n = 11$) temporal biliary drainage. Because the patient in the remaining case was in poor condition and hemorrhaged intraoperatively, he received only a T-tube placement and succumbed 2 days later due to multiorgan failure. During follow-up periods ranging from 1 week to 15 months (median, 6 months), 11 cases survived uneventfully with no evidence of recurrent bleeding (no follow-up data were available for the other four cases).

Table 1. Pseudoaneurysm of the cystic artery due to cholecystitis

First author[Ref.]	Year	Age (years)	Sex	Quincke's triad			Pseudoaneurysm		Gallstone		Treatment		Follow-up
				Abdominal pain	Jaundice	GI bleeding	Localization	Size	Number	Impaction in the neck	Cholecystectomy	Biliary drainage	
Hakami[12]	1976	56	M	Yes	Yes	Yes	External	Nut size	Single	No	Yes	Kehr tube	3 weeks; uneventful
Reddy[13]	1983	61	M	Yes	Yes	Yes	External	3cm	Multiple	No	Yes	T-tube	ND
Rhee[14]	1987	73	M	Yes	No	No	External	ND	ND	ND	Yes	No	One week; uneventful
Wu[15]	1988	64	M	Yes	Yes	Yes	External	4cm	Single	Yes	Yes	T-tube	6 weeks; uneventful
Strickland[16]	1991	72	F	Yes	No	Yes	External	Small	Single	Yes	Yes	No	6 months; uneventful
Barba[17]	1994	70	M	Yes	No	Yes	Internal	2cm	Single	No	Yes (after TAE)	No	6 weeks; uneventful
Nakajima[18]	1996	72	M	Yes	Yes	Yes	Internal	3cm	Multiple	No	Yes	No	6 months; uneventful
England[19]	1998	71	F	Yes	Yes	Yes	Internal	ND	Single	No	No	T-tube	2 days; dead
Kaman[20]	1998	32	F	Yes	Yes	Yes	External	1cm	Multiple	No	Yes	No	12 months; uneventful
Maeda[21]	2002	62	M	Yes	Yes	Yes	Internal	ND	Single	No	Yes (after TAE)	No	15 months; uneventful
Gutierrez[22]	2004	66	F	Yes	No	Yes	External	ND	Single	Yes	Yes	No	ND
Morioka[23]	2004	43	M	No	Yes	Yes	Internal	3cm	Multiple	No	Yes	No	3 weeks; uneventful
Lee[24]	2006	72	F	Yes	No	Yes	Internal	ND	No	No	Yes	No	2 weeks; uneventful
Sibulesky[25]	2006	72	M	Yes	Yes	Yes	Internal	ND	No	No	Yes	No	ND
Joyce[26]	2006	58	M	Yes	No	Yes	Internal	0.2cm	No	No	Yes	No	ND
Present case	2006	58	M	Yes	Yes	Yes	Internal	2cm	Single	Yes	Yes	Nasobiliary tube	12 months; uneventful

GI, gastrointestinal; ND, not described; TAE, transcatheter arterial embolization

In the present case, the impacted gallstone was present synchronously with a pseudoaneurysm of the cystic artery. In addition to acute inflammation, severe damage to the gallbladder wall by the gallstone may have accelerated the formation of the pseudoaneurysm. Although the detailed mechanism by which acute cholecystitis may lead to a pseudoaneurysm formation is not known, we hypothesized that with the inflammatory process, a partial erosion of the serosa and elastic and muscular components of the arterial wall contributed to the pseudoaneurysm of the cystic artery. On the other hand, the likelihood of the inflammation process leading to early thrombosis of the pseudoaneurysm in most cases may explain the rarity of this entity.[15,17]

The patient had a past history of a sclerotic kidney, which is characterized by sclerosis of the arterioles (such as proliferative endarteritis and fibrinoid necrosis) due to long-term persistence of hypertension. Although speculative, it is possible that the nephrosclerosis observed in this case was associated with the aneurysmal formation of the cystic artery.

US and CT have been recognized as highly effective diagnostic tools for detecting pseudoaneurysms, and color-Doppler US can provide further information for diagnosis.[12-26] Nonetheless, these imaging modalities were not diagnostic in the present case because a nearby gallstone and massive intracholecystic hematoma obscured the presence of the pseudoaneurysm. Instead, dynamic MRI was useful for its detection. Selective hepatic angiography can visualize the pseudoaneurysm directly and allow for a definitive diagnosis. Moreover, its diagnostic value is enhanced by the possibility of performing a subsequent therapeutic option. Although transcatheter arterial embolization (TAE) for a cystic artery pseudoaneurysm developing after cholecystectomy is considered to be a definitive therapy,[5-8] in cases of cholecystitis-related pseudoaneurysms (like the present case), this procedure should only be considered as a temporary treatment before a cholecystectomy. Our patient remained hemodynamically stable during the course, and since the pseudoaneurysm of the cystic artery was already diagnosed by dynamic MRI, angiography was not performed. Nevertheless, since hemodynamic stability does not always suggest an arrest of bleeding, preoperative TAE should thus have been performed in the present case to ensure the patient's safety.

The imaging resolution ability of recent multidetector row computed tomography (MDCT) compares favorably with that of dynamic MRI. Therefore, the diagnostic value of MDCT should be explored further in the diagnosis of cystic artery pseudoaneurysm.

Pseudoaneurysmal location can influence the selection of an appropriate surgical procedure: In cases with pseudoaneurysm outside the gallbladder, the careful mobilization of the gallbladder from the liver bed and hepatoduodenal ligament is mandatory because this procedure can directly damage the fragile wall of the pseudoaneurysm. In contrast, in cases with intracholecystic pseudoaneurysm (as in the present case), the occurrence of such injury may be less likely.

In conclusion, our review of the literature indicates that although a pseudoaneurysm of the cystic artery is very rare, it should be included in the differential diagnosis of hemobilia. A cholecystectomy and a ligation of the cystic artery (with or without temporal biliary drainage) are together the mainstay treatment. The proximal control of the hepatic artery (i.e. encirclement of the proximal hepatic artery in preparation for temporal vascular clamping) may be mandatory in order to avoid serious and uncontrollable bleeding.[14] Once the pseudoaneurysm is confirmed, its embolization before a cholecystectomy (which can be attempted laparoscopically) should be done to ensure the patient's safety.[17,21,27,28]

References

1. Sandblom P. Hemorrhage into the biliary tract following trauma: "traumatic hemobilia". Surgery 1948;24:571–86.
2. Sandblom P, Saegesser F, Mirkovitch V. Hepatic hemobilia: hemorrhage from the intrahepatic biliary tract, a review. World J Surg 1984;8:41–50.
3. Curet P, Baumer R, Roche A, Grellet J, Mercadier M. Hepatic hemobilia of traumatic or iatrogenic origin: recent advances in diagnosis and therapy, review of the literature from 1976 to 1981. World J Surg 1984;8:2–8.
4. Croce MA, Fabian TC, Spiers JP, Kudsk KA. Traumatic hepatic artery pseudoaneurysm with hemobilia. Am J Surg 1994;168: 235–8.
5. Saldinger PF, Wang JY, Boyd C, Lang E. Cystic artery stump pseudoaneurysm following laparoscopic cholecystectomy. Surgery 2002;131:585–6.
6. Zilberstein B, Cecconello I, Ramos AC, Sallet JA, Pinheiro EA. Hemobilia as a complication of laparoscopic cholecystectomy. Surg Laparosc Endosc 1994;4:301–3.
7. Bergey E, Einstein DM, Herts BR. Cystic artery pseudoaneurysm as a complication of laparoscopic cholecystectomy. Abdom Imaging 1995;20:75–7.
8. Halbe S, Ahmed NI, Sundar K, Sathyakumar C. Pseudoaneurysm in gall bladder fossa following laparoscopic cholecystectomy. Indian J Gastroenterol 1999;18:122.
9. Mori M, Kohzaki S, Makino K, Amamoto Y, Mori M, Kanbara C, et al. Spontaneous intracholecystic hemorrhage due to polyarteritis nodosa. J Comput Assist Tomogr 1998;22:730–1.
10. Laing FC, Frates MC, Feldstein VA, Goldstein RB, Mondro S. Hemobilia: sonographic appearances in the gallbladder and biliary tree with emphasis on intracholecystic blood. J Ultrasound Med 1997;16:537–43.
11. Kaafarani H, Taher A, Haddad MC, Haidar A, Mourad FH. Spontaneous intracholecystic bleeding in a patient with von Willebrand's disease. Gastrointest Endosc 2003;58:809–11.
12. Hakami M, Beheshti G, Amirkhan A. Hemobilia caused by rupture of cystic artery aneurysm. Am J Proctol 1976;27:56–7.
13. Reddy SC. Pseudoaneurysm of cystic artery with upper gastrointestinal hemorrhage. South Med J 1983;76:85–6.
14. Rhee JW, Bonnheim DC, Upson J. Cystic artery pseudoaneurysm. N Y State J Med 1987;87:47.

15. Wu TC, Liu TJ, Ho YJ. Pseudoaneurysm of the cystic artery with upper gastrointestinal hemorrhage. Case report. Acta Chir Scand 1988;154:151–2.
16. Strickland SK, Khoury MB, Kiproff PM, Raves JJ. Cystic artery pseudoaneurysm: a rare cause of hemobilia. Cardiovasc Intervent Radiol 1991;14:183–4.
17. Barba CA, Bret PM, Hinchey EJ. Pseudoaneurysm of the cystic artery: a rare cause of hemobilia. Can J Surg 1994;37:64–6.
18. Nakajima M, Hoshino H, Hayashi E, Nagano K, Nishimura D, Katada N, et al. Pseudoaneurysm of the cystic artery associated with upper gastrointestinal bleeding. J Gastroenterol 1996;31: 750–4.
19. England RE, Marsh PJ, Ashleigh R, Martin DF. Case report: pseudoaneurysm of the cystic artery: a rare cause of haemobilia. Clin Radiol 1998;53:72–5.
20. Kaman L, Kumar S, Behera A, Katariya RN. Pseudoaneurysm of the cystic artery: a rare cause of hemobilia. Am J Gastroenterol 1998;93:1535–7.
21. Maeda A, Kunou T, Saeki S, Aono K, Murata T, Niinomi N, et al. Pseudoaneurysm of the cystic artery with hemobilia treated by arterial embolization and elective cholecystectomy. J Hepatobiliary Pancreat Surg 2002;9:755–8.
22. Gutierrez G, Ramia JM, Villar J, Garrote D, Ferron A, Ruiz E. Cystic artery pseudoaneurysm from an evolved acute calculous cholecystitis. Am J Surg 2004;187:519–20.
23. Morioka D, Ueda M, Baba N, Kubota K, Otsuka Y, Akiyama H, et al. Hemobilia caused by pseudoaneurysm of the cystic artery. J Gastroenterol Hepatol 2004;19:724–6.
24. Lee JW, Kim MY, Kim YJ, Suh CH. CT of acute lower GI bleeding in chronic cholecystitis: concomitant pseudoaneurysm of cystic artery and cholecystocolonic fistula. Clin Radiol 2006;61: 634–6.
25. Sibulesky L, Ridlen M, Pricolo VE. Hemobilia due to cystic artery pseudoaneurysm. Am J Surg 2006;191:797–8.
26. Joyce MR, Donnolly M, O'Shea L, Jeffers M, O'Riordain D. Pseudoaneurysm of the cystic artery: a diagnostic dilemma and rare cause of haemobilia. Ir J Med Sci 2006;175:81.
27. Delgadillo X, Berney T, de Perrot M, Didier D, Morel P. Successful treatment of a pseudoaneurysm of the cystic artery with microcoil embolization. J Vasc Interv Radiol 1999;10:789–92.
28. Reber PU, Baer HU, Patel AG, Wildi S, Triller J, Buchler MW. Superselective microcoil embolization: treatment of choice in high-risk patients with extrahepatic pseudoaneurysms of the hepatic arteries. J Am Coll Surg 1998;186:325–30.

Dig Dis Sci (2007) 52:3191–3198
DOI 10.1007/s10620-006-9254-6

Duodenal Gastrointestinal Stromal Tumor Adjacent to the Minor Papilla with Concomitant Pancreatic Divisum

Tomotaka Akatsu · Koichi Aiura · Shigeyuki Kawachi · Minoru Tanabe · Motohide Shimazu · Masakazu Ueda · Kaori Kameyama · Masaki Kitajima

Received: 31 December 2005 / Accepted: 8 February 2006 / Published online: 19 April 2007

Keywords Gastrointestinal stromal tumor · Duodenum · Duodenectomy · Minor duodenal papilla.

Introduction

Gastrointestinal stromal tumors (GISTs) are the most common mesenchymal tumor of the gastrointestinal tract. These tumors occur along the entire length of the gastrointestinal tract, but with different frequencies at different anatomic locations. These tumors develop most commonly in the stomach (50%), followed by the small bowel (25%) [1–3]. The colon (10%), omentum/mesentery (7%), and esophagus (5%) are less common primary sites. Only a few GISTs develop in or adjacent to an orifice of the main pancreatic duct [4–7]. Here we report a unique case of GIST occurring adjacent to the minor duodenal papilla with concomitant pancreatic divisum (the majority of exocrine flow is routed through the minor duodenal papilla). This patient was treated successfully by minor papilla-sparing partial duodenectomy with placement of a stent tube in the minor papilla.

Case Report

A 70-year-old man was referred to our hospital for examination and treatment for severe anemia. On admission, his blood hemoglobin level was 5.6 g/dl, and the serum levels of carcinoembryonic antigen and carbohydrate antigen 19-9 tumor markers were within normal limits. His medical history was unremarkable. The abdomen was soft and not distended, with mild tenderness in the upper abdomen. The rest of the physical examination was normal. Colonoscopy did not demonstrate any bleeding sites. Upper gastrointestinal endoscopy disclosed a submucosal tumor with bleeding from a central umbilication within the second portion of the duodenum (Figure 1A). The tumor location corresponded to the minor duodenal papilla. Bleeding was arrested using argon plasma coagulation. Hypotonic duodenography showed a mass protruding into the duodenal lumen (Figure 1B). Computed tomography (CT) images showed a 3-cm, hypodense mass with heterogeneous contrast enhancement (Figure 2). No regional lymph node metastases or distant metastases were identified. Magnetic resonance (MR) imaging and endoscopic ultrasonography were performed to evaluate involvement of the surrounding structures. T1-weighted MR imaging showed a 2.8-cm, well-demarcated, homogeneous hypointense tumor around the head of the pancreas (Figure 3A). Postcontrast T2-weighted MR imaging demonstrated peripheral contrast enhancement and internal cystic degeneration (Figure 3B). No involvement of the surrounding structures was observed. Endoscopic ultrasonography demonstrated a 3.1-cm, smooth, well-demarcated, and hypoechoic mass with central hyperechoic areas (Figure 4). The tumor was present outside the pancreas. MR cholangiopancreatography showed that the main pancreatic duct was draining into the minor papilla (Figure 5A). Endoscopic retrograde pancreatography through the major papilla showed only the duct of Wirsung, and cannulation into the minor papilla was unsuccessful (Figure 5B). Angiography was performed to investigate vascular anatomy and anomaly in preparation for tumor resection as well as to

T. Akatsu · K. Aiura (✉) · S. Kawachi · M. Tanabe · M. Shimazu · M. Ueda · M. Kitajima
Department of Surgery, Keio University School of Medicine, 35 Shinanomachi, Shinjyuku-ku, Tokyo, 160-8582 Japan
e-mail: aiurako@sc.itc.keio.ac.jp

K. Kameyama
Division of Diagnostic Pathology, Keio University School of Medicine,
Tokyo, Japan

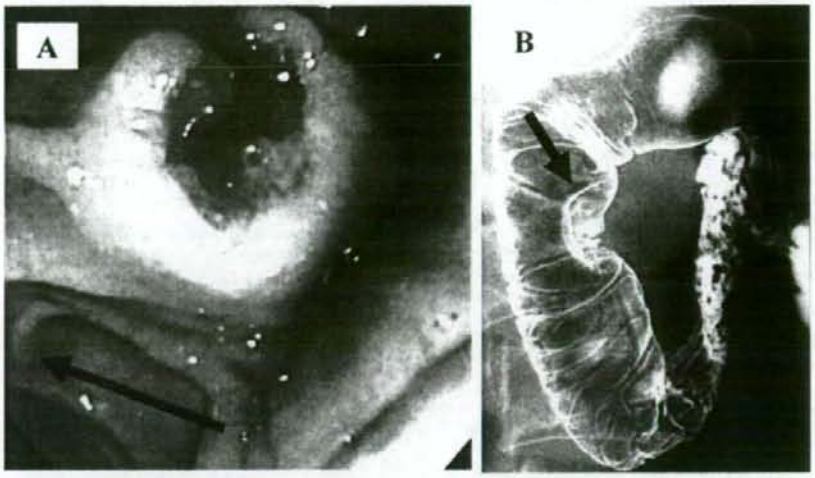

Fig. 1 Duodenal gastrointestinal stromal tumor. (A) Endoscopic view of bleeding from a central umbilication of the tumor, which was located at the oral side of the ampulla of Vater (arrow). (B) Hypotonic duodenography demonstrating a mass (arrow) protruding into the duodenal lumen

examine tumor vascularity. Selective abdominal angiography (via the celiac and supramesenteric arteries) revealed a tumor stain originating from the anterior and posterior superior pancreaticoduodenal arteries (Figure 6). No major vascular anomaly was identified.

Microscopically, preoperative biopsy samples via upper gastrointestinal endoscopy were composed predominantly of spindle-shaped cells with a fascicular or storiform growth pattern. These cells immunostained positively for c-kit and CD34, and negatively for S-100 protein, smooth muscle actin, and desmin. The mitotic count of the cells was <5/50 high-power fields (HPF). Histological examination of the biopsy samples resulted in a diagnosis of low-risk GIST (tumor <5 cm and mitotic count <5/50 HPF) [8, 9].

Pancreaticoduodenectomy was proposed before surgery to remove the tumor. At the time of laparotomy, the firm mass projected from the anterior wall of the second portion of the duodenum. Involvement of adjacent organs such as the pancreas or regional lymph nodes was not observed. Inspection of the peritoneal surfaces and liver revealed no metastasis. To identify the origin of the tumor accurately, the duodenal wall was opened from its ventral margin. The tumor was found nearly adjacent to the minor papilla but separated slightly from it. After the second portion of the duodenum was skeletonized off the pancreas to gain the medial margin, the tumor was resected carefully along the tumor edge (wedge resection) with a margin of safety and with an intact tumor capsule (Figure 7A). The extent of the resected duodenum was approximately 50% of the wall. Although the

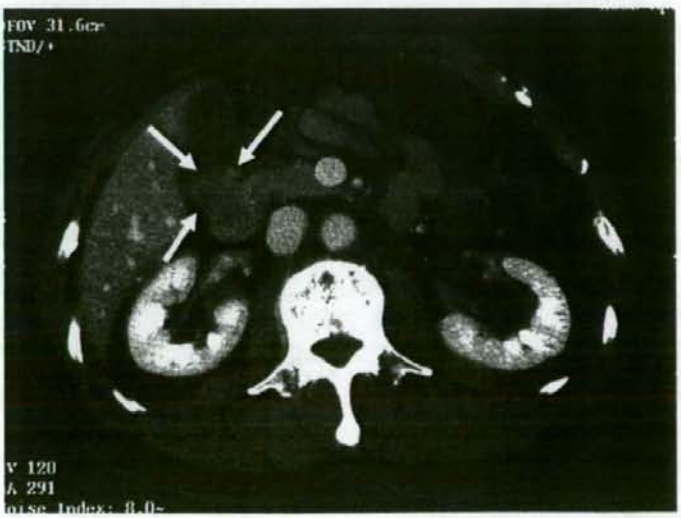

Fig. 2 Computed tomography scan of a 3-cm, hypodense mass that displayed heterogeneous contrast enhancement (arrows)

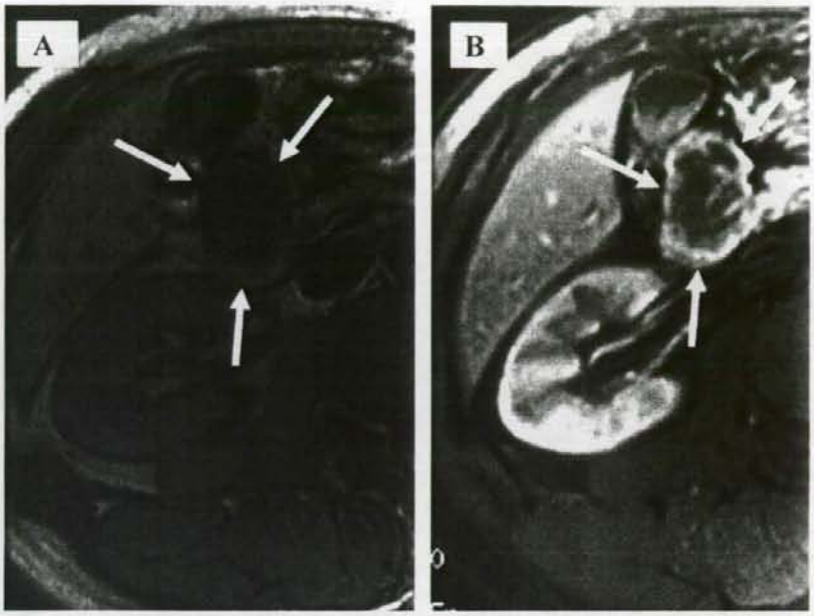

Fig. 3 Magnetic resonance imaging characterization. (A) T1-weighted image of a 2.8-cm, well-demarcated, homogeneous hypointense tumor (arrows). (B) A postcontrast T2-weighted image showing peripheral contrast enhancement and internal cystic degeneration (arrows)

minor duodenal papilla was preserved, the resection margin was close enough to risk scarring stenosis of this orifice. Therefore, following gradual dilation of the orifice to 0.9 mm using a series of bougies (from 0.1 to 0.9 mm), a stent tube (4-Fr atom tube) was inserted into the minor papilla. The remnant duodenum was closed horizontally with Gambee single interrupted suturing (Figure 7B). Lymphadenectomy was not performed.

The resected specimen consisted of an encapsulated solid mass 3 cm in diameter. The tumor developed intramurally, and its cut surface was tan in color with central cystic components (Figure 8A). The margins of resection were

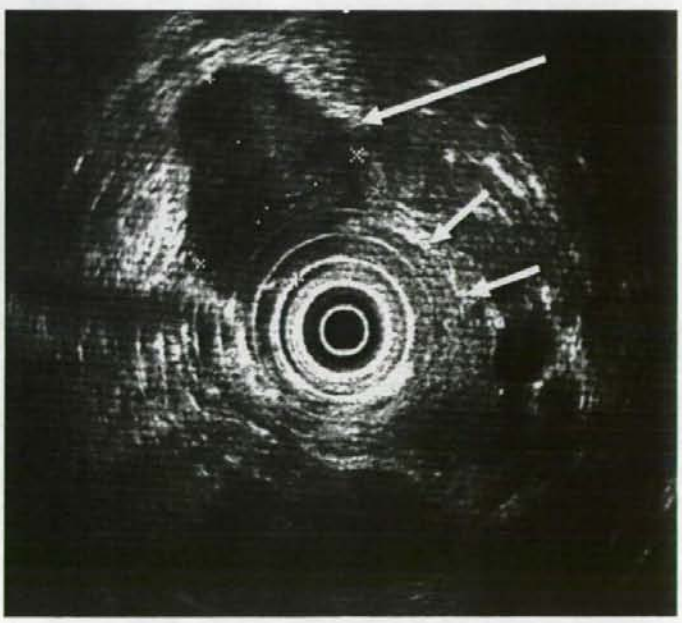

Fig. 4 Endoscopic ultrasonographic image of a 3.1-cm, well-demarcated, hypoechoic mass (long arrow) with central hyperechoic areas located outside the pancreas (short arrows)

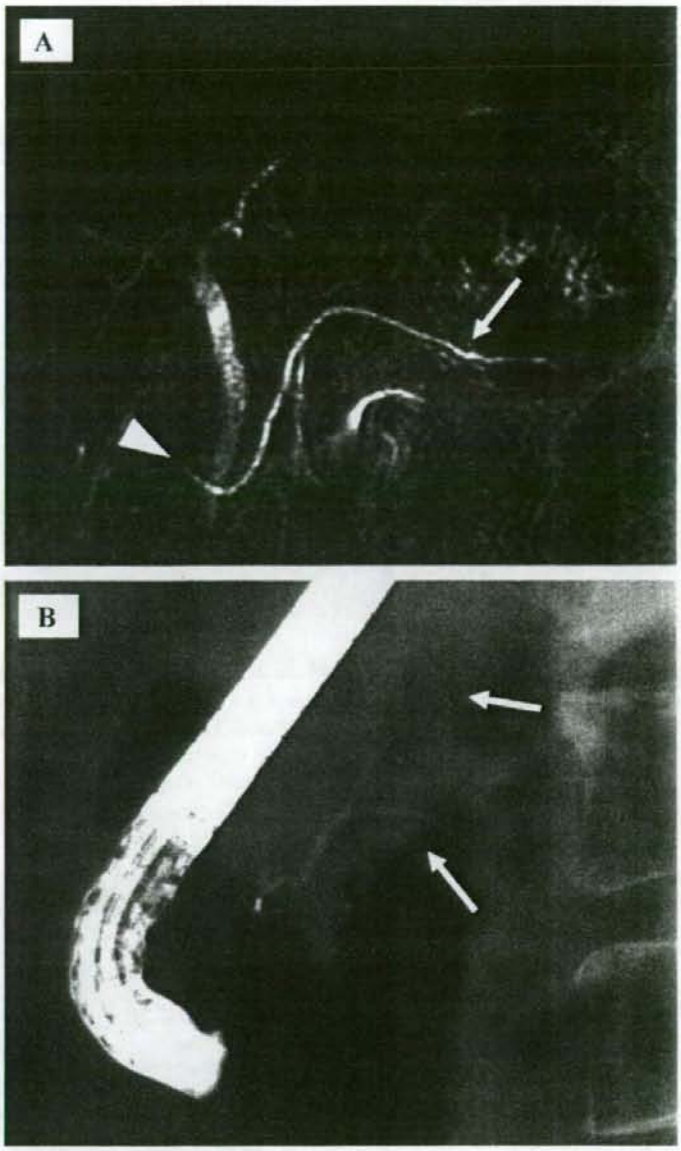

Fig. 5 Pancreatic divisum. (A) MR cholangiopancreatography demonstrating that the main pancreatic duct (arrow) was routed through the minor duodenal papilla (arrowhead). (B) Endoscopic retrograde pancreatographic image. Injection of the major papilla resulted in filling of the duct of Wirsung, which terminates with arborization (arrows) in the pancreatic head without filling the dorsal pancreatic duct. Cannulation into the minor papilla was unsuccessful

confirmed to be free by microscopy. Microscopic findings and immunohistochemical staining patterns of the resected specimen were compatible with those of the biopsy samples (Figures 8B–D). The tumor showed infrequent mitotic figures (<5/50 HPF), and the Ki-67 labeling index was less than 1%. Based on these findings, the tumor was diagnosed as a low-risk GIST [8, 9]. Adjuvant chemotherapy was not recommended. Gastroduodenography 1 week after the surgery did not demonstrate any abnormal findings (such as stenosis and leakage). The patient's postoperative course was uneventful. To prevent postoperative impairment of sphincter function of the minor papilla due to long-term dilation and stenting, the stent tube was removed endoscopically 2 months later (Figure 9). The patient has survived for 5 months without evidence of recurrence.

Discussion

We have reported a very rare case of GIST occurring adjacent to the minor duodenal papilla with concomitant pancreatic

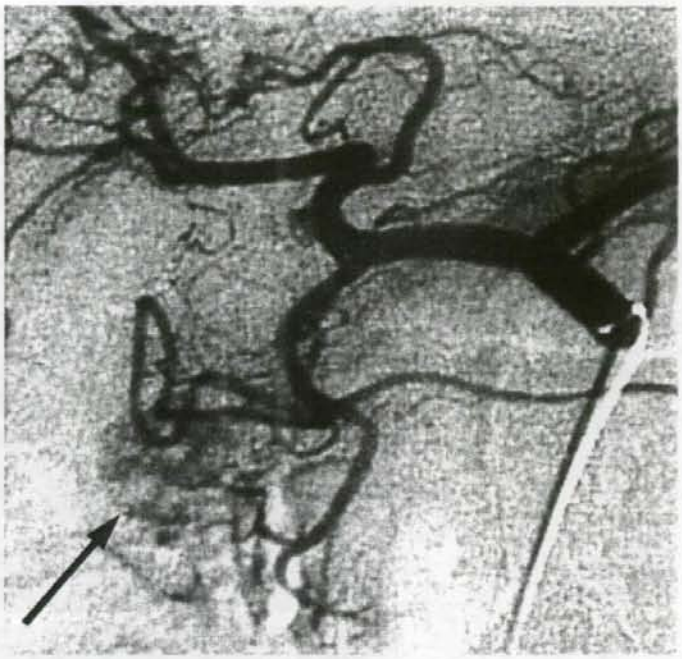

Fig. 6 Selective abdominal angiography via the celiac artery revealed a tumor stain (arrow) originating from the anterior and posterior superior pancreaticoduodenal arteries

divisum. No previous reports of this unusual condition were identified in a Pubmed search of literature from January 1950 to November 2005 using the key words GIST, duodenum, minor duodenal papilla, and pancreatic divisum.

The patient described here was a 70-year-old man. GISTs can develop at any age, although they are more common in elderly adults, with a peak incidence in the fifth and sixth decades of life [10, 11]. It appears that men and women are affected equally. This patient presented with severe anemia caused by gastrointestinal bleeding. Presenting symptoms of duodenal GISTs include abdominal pain, nausea, dyspepsia, gastrointestinal bleeding (including melena, hematemesis, and anemia), or intra-abdominal hemorrhage [4–7, 12–14]. Small GISTs may be detected incidentally during routine follow-up for other diseases or screening examinations, or at the time of laparotomy.

In patients with primary GISTs who demonstrate no evidence of metastasis, surgical resection is the main treatment [2, 3]. However, the optimal surgical procedure for duodenal GISTs remains undefined. A variety of techniques, including local excision, partial duodenectomy, pancreas-sparing duodenectomy, and pancreatoduodenectomy, has been described, according to the size and location of the tumor [4–7, 12–14].

There are several principles of surgical treatment for resectable GISTs [14–17]. First, the primary goal is complete gross resection with negative microscopic margins. Second, lymphadenectomy is not necessary because lymph node metastases rarely occur. Third, the tumor should be handled with care to avoid rupture, since tumor seeding may ensue if the capsule is torn. Although the tumor presented here was located adjacent to the minor duodenal papilla, complete resection with negative microscopic margins and with an intact capsule was achieved by partial duodenectomy with preservation of the minor papilla. Postoperative gastroduodenography demonstrated that the anastomotic site was not stenosed, and the patient has survived for 5 months without evidence of recurrence. Although the follow-up period of this patient has been short, this procedure could prove to be a successful substitute for the more invasive pancreatoduodenectomy. Nonetheless, because there is a risk of subsequent anastomotic stenosis development, as well as later tumor recurrence, long-term follow-up with endoscopic and radiological examinations will be required.

Pancreas divisum is a rare anatomical anomaly in which the ventral and dorsal pancreatic ducts fail to unite during embryonic development. In the present patient displaying this defect, the majority of exocrine flow was routed through the minor duodenal papilla. Postoperative obstruction of the minor papilla would lead to the development of pancreatitis, thus the patency of its orifice was very important. Therefore, at surgery, the orifice of the minor papilla was gradually dilated to 0.9 mm using a series of bougies

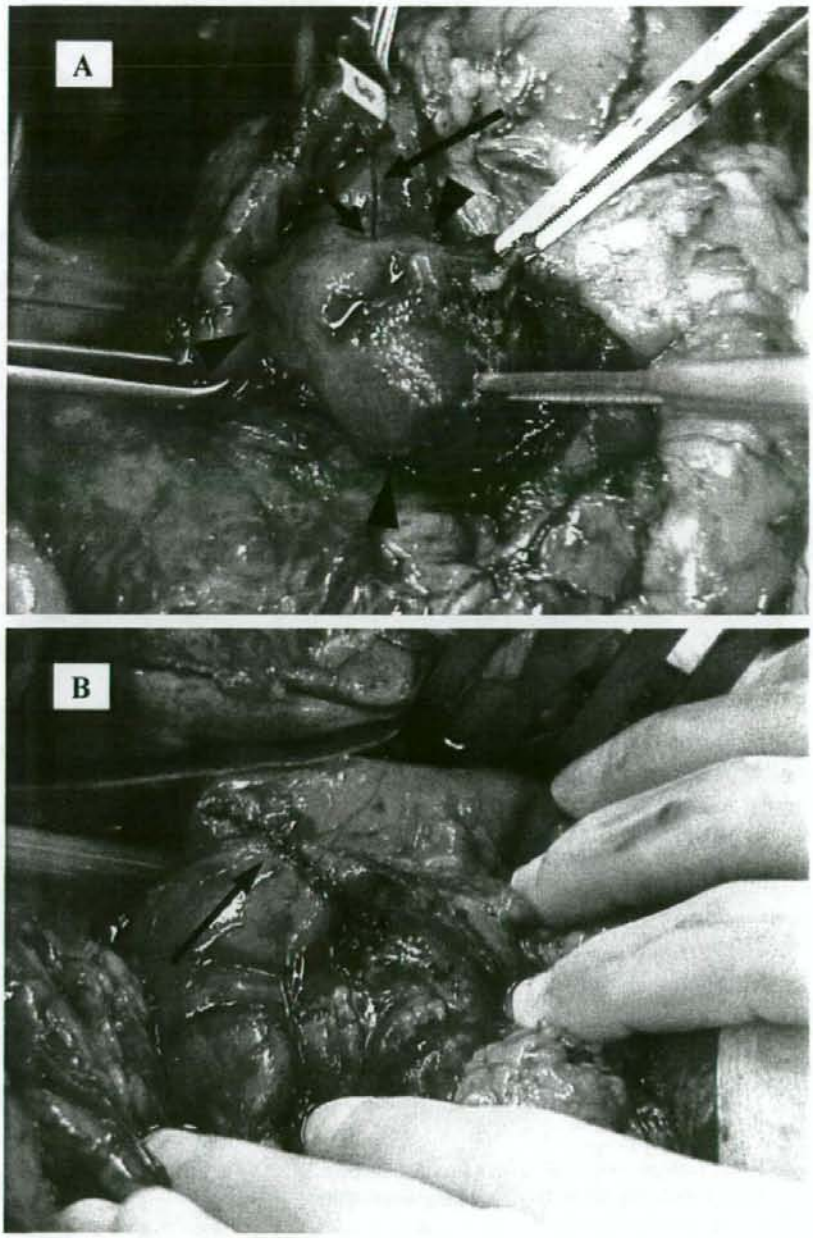

Fig. 7 Operative field photographs. (A) The tumor with a central umbilication (arrowheads) was located adjacent to the minor papilla (short arrow). The tumor was resected carefully along the tumor edge with a margin of safety (wedge resection). Following gradual dilation of the orifice to 0.9 mm using a series of bougies (from 0.1 to 0.9 mm) (long arrow), a stent tube (4-Fr atom tube) was inserted into the minor papilla. (B) The remnant duodenum was closed horizontally with Gambee single interrupted suturing (arrow)

(from 0.1 to 0.9 mm), and a stent tube (4-Fr atom tube) was placed in it. The tube was removed 2 months later, but this patient did not develop hyperamylasemia or pancreatitis subsequently.

In the present case, the tumor margin was determined by intraoperative macroscopic examination. If the final specimen margin had been positive, additional surgery (e.g., pancreaticoduodenectomy) would have been required.

In conclusion, we have reported a very rare case of GIST adjacent to the minor duodenal papilla with concomitant pancreatic divisum. Although pancreatoduodenectomy was proposed preoperatively, complete resection with negative

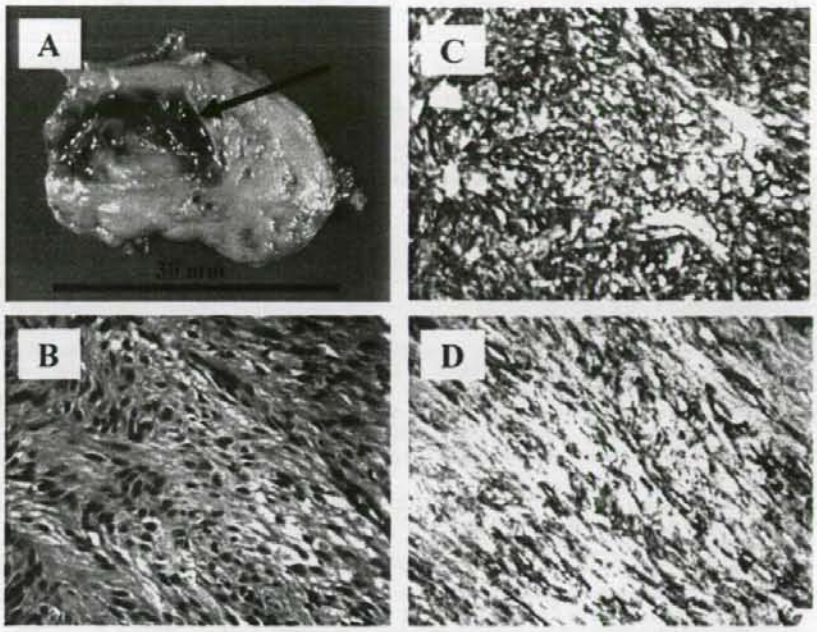

Fig. 8 (A) The resected tumor specimen was tan in color with central cystic degeneration (arrow). (B) The tumor was composed of spindle-shaped cells showing fascicular growth. (C) The tumor cells showed positive staining for c-kit. (D) These cells stained positive for CD34. (Original magnifications: B–D, × 200)

Fig. 9 Endoscopic view of the anastomosis after endoscopic removal of the stent tube placed in the minor papilla. Note that the suture strings (short arrows) were adjacent to both the ampulla of Vater (arrowhead) and the minor papilla (long arrow)